Photonic-Assisted Arbitrary Waveform Generation for Uplink Applications in Beyond 5G Taking Advantage of Low Frequency Technology

Tsuyoshi Konishi, *Senior Member, IEEE*, Yuta Kaihori, and Masayuki Makino

(Invited Paper)

***Abstract*—We present a photonic-assisted arbitrary waveform generation for uplink applications in beyond 5G taking advantage of low frequency technology and it has a potential to upgrade signal frequency from MHz to more than tens GHz retaining the high ENOB of conventional low frequency electrical technology competitive to the state of the arts of tens GHz class AWG. In machine-to-machine communications over uplink traffic as one of application scenario examples, massive multi-data should be accommodated and be conveyed to beyond GHz region in the era of beyond 5G. The proposed photonic assistance for temporal waveform compression has a potential to upgrade signal frequency from MHz to more than tens GHz retaining the high ENOB of the low frequency technology and surpass the state of the arts of tens GHz class AWG. We successfully demonstrate the principle of the proposed approach in experiment and the potential of achievable ENOB over 12 bit at 50 GHz in simulation.**

***Index Terms*—Arbitrary waveform generator, beyond 5G, digital-to-analog converter, massive machine-to-machine communications, optical signal processing.**

I. Introduction

TO BREAK through various barriers in the mobile fifth generation (5G) and beyond 5G, it is said that untapped resources and technologies should be re-examined from the earliest stages of design [1]. Ultra-wideband carriers have a large impact on baseband (BB) processing systems, especially digital-to-analog converters (DACs) and analog-to-digital converters (ADC) [2]. With an eye on the future demand on such extreme wideband carriers, various photonic approaches for DAC and ADC have been pursued thus far [3]–[9]. We have also investigated several photonic approaches for ADC [10]–[19] and DAC [20]. For example, new services offered by 5G and beyond 5G enlarges the uplink to downlink ratio, related to the increasing accessibility demand of cloud services from massive machine-to-machine (M2M) communications over uplink traffic [21], [22]. Multiple data from massive users share the same radio resources and is multiplexed in an orthogonal frequency division multiplexing (OFDM) signal. Such an OFDM signal must be migrated to that in beyond-GHz region, and ROF-based uplink requires a high-performance arbitrary waveform generator (AWG) offered by GHz-class electrical DACs. However, several issues, including the analog resolution, cost, and power consumption become critical as the signal frequency rises beyond GHz [23]. Photonic AWGs using the spectral-domain and time-domain spectral shapers (SDSS and TDSS) are well-investigated [24]–[29] and are originally used for ultrafast optical arbitrary waveform synthesis. Although they can provide THz-class ultrafast optical signals, which are electrically impossible to generate, there are still issues that need to be resolved for the 5G and beyond 5G applications. SDSS exhibit some issues in spectral shaping devices, including the limited spectral resolution, slow refresh rate, bulky size, and high cost [28]. TDSS has a close relationship with photonic time stretch technique which is usually considered to be used in ADC to reduce the requirement of sampling rate by stretching the signal [30], [31]. After stretching the signal, an electrical modulator can treat it as a time-domain spectral shaper. Most TDSS aim at the THz-class ultrafast optical signal generation after Fourier transform using dispersion, but it is not suitable for the next-generation GHz-class signals in 5G and beyond 5G applications. An unbalanced architecture has been proposed to apply TDSS to GHz-class microwave frequency multiplication, instead of THz-class ultrafast optical signal generation [32], [33]. However, since all previous schemes rely on the GHz-class electrical technology, the inherent issues of analog resolution, cost, and power consumption remain pertinent. Since the root of the above issues emerges from the technical limits of the state-of-the-art GHz-class electrical technology, the AWG development cannot overcome the trade-off relationship among the above issues as long as it relies on the GHz-class electrical technology.

In this paper, we propose a photonic-assisted AWG for uplink applications in beyond 5G using the advantage of matured MHz-class low-frequency technology, which can provide overwhelming competitiveness in analog resolution, cost, and

Manuscript received 31 March 2022; revised 19 May 2022 and 18 June 2022; accepted 20 June 2022. Date of publication 24 June 2022; date of current version 21 October 2022. These research results were obtained from the commissioned research for the research project "MTMT B5G" by National Institute of Information and Communications Technology (NICT), Japan. *(Corresponding author: Tsuyoshi Konishi.)*

The authors are with the Graduate School of Engineering, Osaka University, Suita 565–871, Japan (e-mail: konishi@mls.eng.osaka-u.ac.jp; y.kaihori@ap.eng.osaka-u.ac.jp; m.makino@ap.eng.osaka-u.ac.jp).

Color versions of one or more figures in this article are available at https://doi.org/10.1109/JLT.2022.3186038.

Digital Object Identifier 10.1109/JLT.2022.3186038

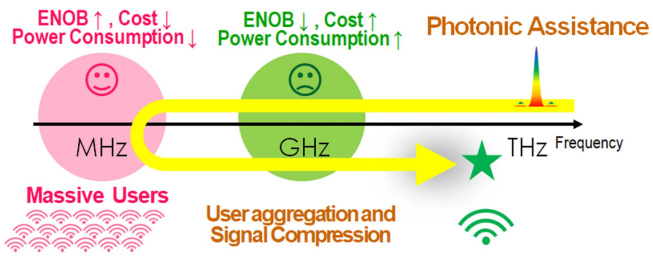

Fig. 1. The conceptual diagram of the proposed photonic-assisted AWG.

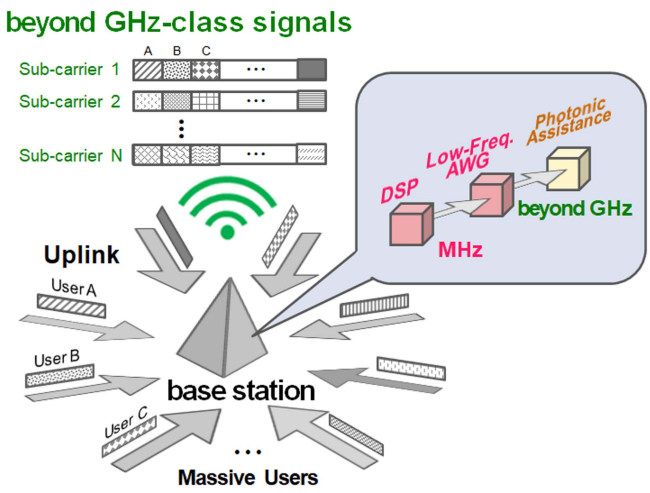

Fig. 2. Application scenario example for massive data and users over uplink traffic and their migration to beyond-GHz region.

power consumption except signal frequency, the only advantage of the GHz-class AWG, as shown in Fig. 1. The point is exploitation of latent benefits in low-frequency technology in beyond-GHz region so that it could be one possible solution in the development of high-frequency AWGs. In our approach, a low-frequency AWG is an essential component to provide benefits in low-frequency technology. To the best of our knowledge, beyond GHz-class AWG using the MHz-class low-frequency technology with photonic assistance based on chirped pulse compression is first proposed to remodel it to obtain competitive performances in signal frequency, as well as analog resolution, cost, and power consumption.

II. Principle of Photonic-Assisted Arbitrary Signal Generation for Uplink Applications in Beyond 5G

A. Application Scenario Example

Here, we take an M2M communication as one of application scenario examples which assumes massive data and users over uplink traffic, as shown in Fig. 2. Data is gathered on a base station from massive users and an OFDM signal is generated so that each user be allocated to each OFDM subcarrier by a digital signal processor (DSP) and an AWG. The data signal is digitally processed for segmentation and tuning so as to accommodate it in the stretched carrier pulse according to the length of signal. The generated OFDM signal is migrated to that in beyond-GHz region with photonic assistance. Since signals become sparse in beyond-GHz region after signal compression, the produced temporal free space in a frame could be used for accommodation. When the number of massive users exceeds that of the OFDM subcarriers, such a produced temporal free space can be used for accommodation of overflowing data and users. In addition, when considering various use cases in beyond 5G [34], a single AWG in each edge subsystem (e.g., Remote Radio Head: RRH) is not required to fill all the temporal free space because a large number of signals from massive edge subsystems should be bundled again and sent to the backhaul. For example, considering several tens GHz RoF based fronthaul serving a large number of users located at different locations within the cell, a large number of signals will be sent to a baseband unit (BBU) pool from edge subsystems like RRHs in the front hall and these signals will be bundled together and sent to the back hall. These signals are bundled again and sent to the backhaul at the BBU pool, where all the space should be finally filled. This requires an additional signal processing for aggregation of multi-data from vast multi-user information. With beyond GHz-class technology complex multi-data aggregation is almost impossible, but with MHz-class low-frequency technology it could be possible. The photonic assistance based on chirped pulse compression only have to convey the processed result with a DSP and an AWG in a MHz-region to beyond-GHz region.

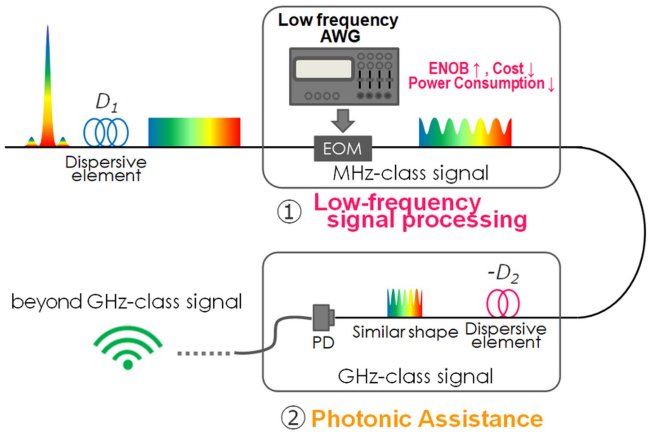

Fig. 3. The proposed configuration for the photonic-assisted GHz-class AWG utilizing the advantages of ENOB, cost, and power consumption in MHz class low frequency technology and chirped pulse compression.

B. Photonic-Assisted Beyond-GHz-Class AWG With Exploitation of Latent Benefits in Low-Frequency Technology

Fig. 3 shows the proposed configuration of the photonic-assisted GHz-class AWG using MHz-class low-frequency AWG and chirped pulse compression. It consists of two components, (1) low-frequency signal processing and (2) photonic assistance. The performance of the proposed photonic-assisted beyond-GHz-class AWG essentially relies on the advantages of the used MHz class low frequency AWG. While the power consumption of AWG in the region over several tens GHz for beyond 5G at least exceeds several hundred W, that of the proposed

system in low-frequency region does not exceed it including additional active components such as optical modulators and erbium doped-fiber-amplifiers (EDFAs). In fact, USB powered optical devices such as a EDFA (e.g., AEDFA-13 Mini, amonics) comes to be available whose power consumption is less than a few tens W. We used the MHz region as a working space because AWGs in this region are free from the mentioned issues except frequency. It consists of two different linear dispersive elements with different dispersion amounts of D_1 and D_2, a low-frequency EO modulator, an MHz-class electrical AWG, and a high-frequency PD. While this asymmetric configuration aims at the microwave frequency tunability using the GHz-class electrical technology [32], [33], our proposed configuration aims at solving the above issues employing the advantages of the MHz-class low-frequency electrical technology [35], [36]. In our scheme, the seed pulse is first stretched by a dispersive element with the dispersion amount of D_1 for wavelength-to-time mapping in the MHz region, which converts the temporal waveform of a seed optical pulse into a longitudinal mapped spectrum wave as a result of an approximate Fourier transform. A photonic time stretch technique is well known and it can achieve wavelength-to-time mapping using wavelength dispersion [37] and it is used just before the part of (1) low-frequency signal processing in our scheme in Fig. 3. Since it enables for the optical pulse spectrum to be transformed to the corresponding temporal waveform, it can be used for a high-speed spectroscopic technique [38]. In addition, when a wide-bandwidth RF waveform is superimposed on the stretched optical pulse via an E/O modulator, its ultrafast temporal waveform can be stretched furthermore so that the subsequent narrow bandwidth electrical receiver could treat it [39]. The optical spectral shape mapped along with the longitudinal temporal direction can be modulated using a low-frequency EO modulator and an electrical AWG in the MHz region. When a seed optical pulse with an unmodulated initial spectrum (e.g., a rectangle shape spectrum) is prepared as a long pulse of sub-μs temporal width, an arbitrary electrical waveform can be superimposed on the optical spectral shape mapped along with the longitudinal temporal direction, ideally as it is. The modulated optical spectrum is subsequently compressed by the 2nd dispersive element with a dispersion amount of D_2 different from the 1st dispersive element. The frequency of the modulated analog signal is raised by $D_1/(D_1 + D_2)$ times. Since the mapped waveform is analogously preserved as a similar compressed version of the original electrical waveform, it can realize the performance in the GHz region retaining at least the same level as those of the MHz-class electrical AWG. Fig. 4 shows the change in the spectrum of the OFDM signal before and after signal compression. The general OFDM signal E can be written as the following expression.

$$E(t) = \sum_{n=0}^{N-1} [a_n \cos\{2\pi(\nu_c + n\nu_0)t\} - b_n \sin\{2\pi(\nu_c + n\nu_0)t\}] \quad (1)$$

where a_n and b_n are data symbols of the n th subcarrier and ν_c and ν_0 are the carrier frequency and the subcarrier frequency

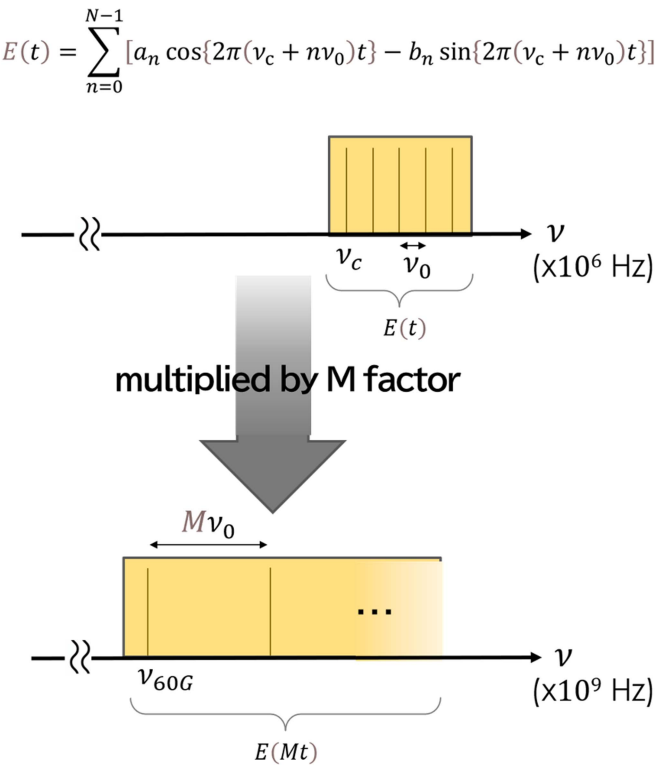

Fig. 4. The proposed asymmetric configuration of the time-domain optical pulse shaping approach for radio frequency or microwave arbitrary waveform synthesis.

interval. After compression, not only the bandwidth but also the carrier frequency will be multiplied by M factor accordingly. Therefore, the superimposed signal before compression should be synthesized so that both the bandwidth and carrier frequency could be adopted to those for beyond 5G after compression. For example, when we assume a 50 GHz-band OFDM signal with a 1GHz frequency interval after 250-fold compression, an original OFDM signal with a 200 MHz carrier frequency and a 4MHz frequency interval should be synthesized. The frequency interval of several MHz is achievable using the current C-FBG technology which can provide sub-micro second pulse with a couple of tens nm bandwidth optical pulse.

III. Experimental Verification

We verified the principle of our approach using a sinusoidal signal and a QPSK-modulated OFDM signal in experiment.

A. Migration of an MHz-Class Signal to That in the GHz Region

We verified preliminary signal compression for the migration of an MHz-class signal to that in the GHz region using a sinusoidal signal. Fig. 5 shows the experimental setup for the preliminary verification of the migration of a MHz-class signal. The short optical pulse from the MLFL (Calmar FPL-M2CFF-OSU-01) is first stretched to the MHz region by a single mode fiber (SMF) with the dispersion amount of 480 ps/nm. Then, the stretched pulse is modulated by a 300-MHz sinusoidal

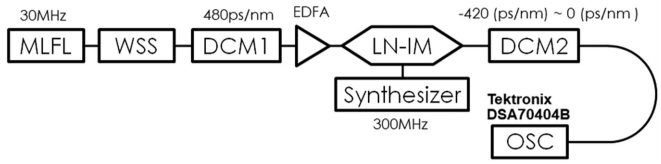

Fig. 5. The proposed asymmetric configuration of the time-domain optical pulse shaping approach for radio frequency or microwave arbitrary waveform synthesis.

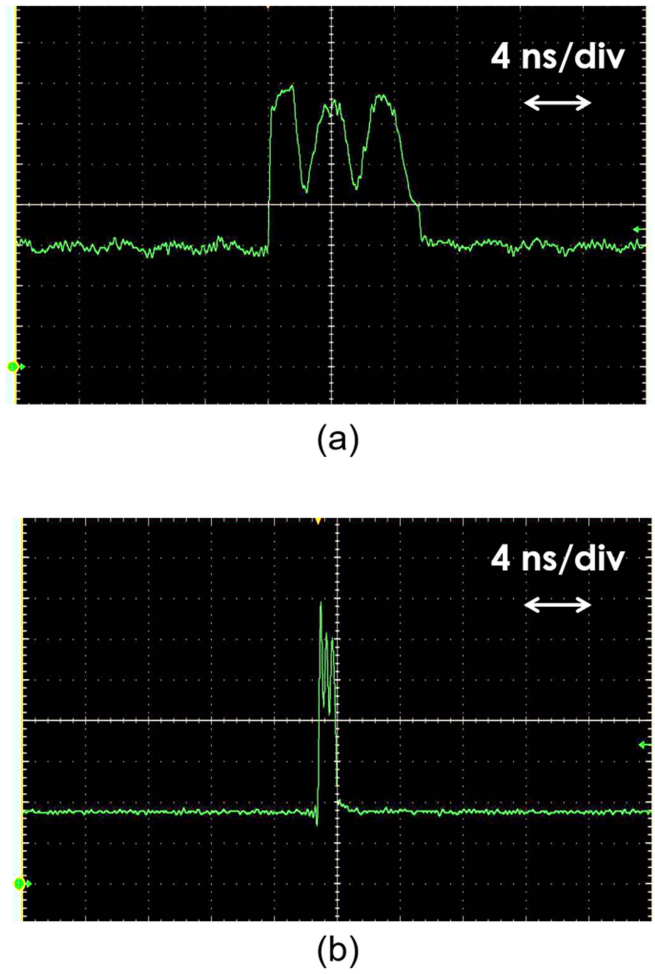

Fig. 6. Experimental results of (a) the waveform generated by superimposing a sinusoidal waveform of 300 MHz and (b) the compressed waveform of 2.4 GHz.

wave. The modulated stretched pulse in the MHz region is subsequently compressed to higher-frequency regions by two dispersion-compensating fibers (DCFs) with a different dispersion of −420 ps/nm.

The generated waveforms are measured by a digital oscilloscope (Tektronix DSA70404B) via a PD. Fig. 6(a) and (b) show the experimental results before and after compression. They agree well with the expected compressed ratio given by 8, and they are compressed from 300-MHz to 2.4-GHz sinusoidal waves, respectively.

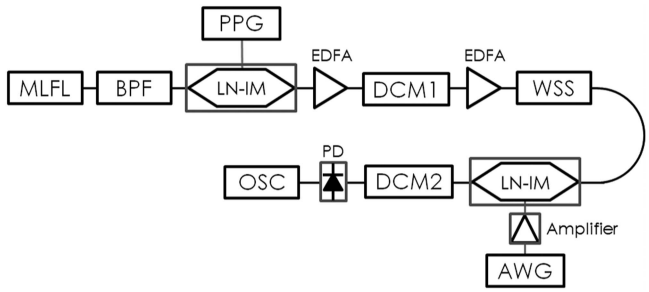

Fig. 7. The proposed asymmetric configuration of the time-domain optical pulse shaping approach for radio frequency or microwave arbitrary waveform synthesis.

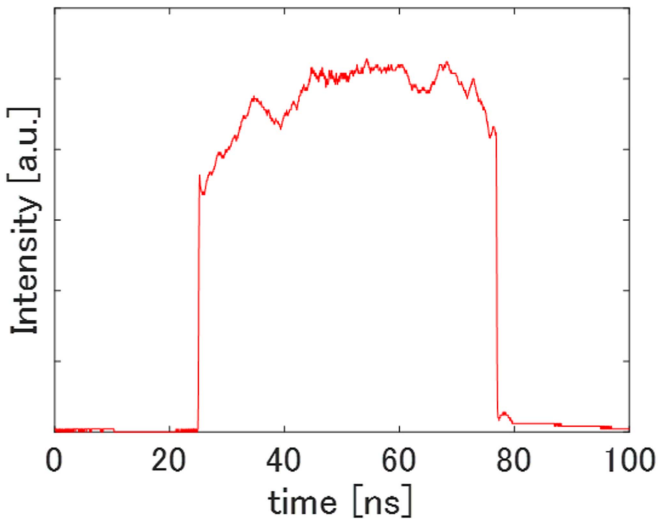

Fig. 8. Measured waveform of stretched pulse before superimposing a signal.

B. Signal Quality Examination After Migration Using QPSK-Modulated Optical OFDM Signal

We examine the signal quality performance during the migration of an MHz-class signal using a QPSK-modulated optical OFDM signal. Fig. 7 shows the experimental setup for the same. The short optical pulse from the MLFL (Calmar FPL-M2CFF-OSU-01) is first frequency-divided via a PPG and a Mach-Zehnder-modulator (MZM) at a frequency division ratio of 1/30 and stretched to MHz region by a single mode fiber with the total dispersion amount of −1970 ps/nm. A PPG-driven MZM extracts pulses at constant temporal intervals, thereby decreasing a repetitive frequency of a pulse train at a frequency division ratio of 1/30 because the maximum synchronous frequency of our AWG is 1 MHz. A QPSK-modulated optical OFDM signal was synthesized and stored in an MHz-class AWG (Tektronix AWG610) and superimposed to the stretched optical pulse through an MZM with an RF amplifier one by one. The stretched pulse is modulated with 256 patterns waveforms corresponding to a QPSK modulated 4-subcarriers whose frequency interval $\nu_0 = 20$ MHz. All 256 waveforms are superimposed via an AWG and a MZM one by one and each waveform is switched after waveform measurement. In this experiment, assuming $\nu_c = \nu_0$ for simplicity in (1), the superimposed signal E corresponds

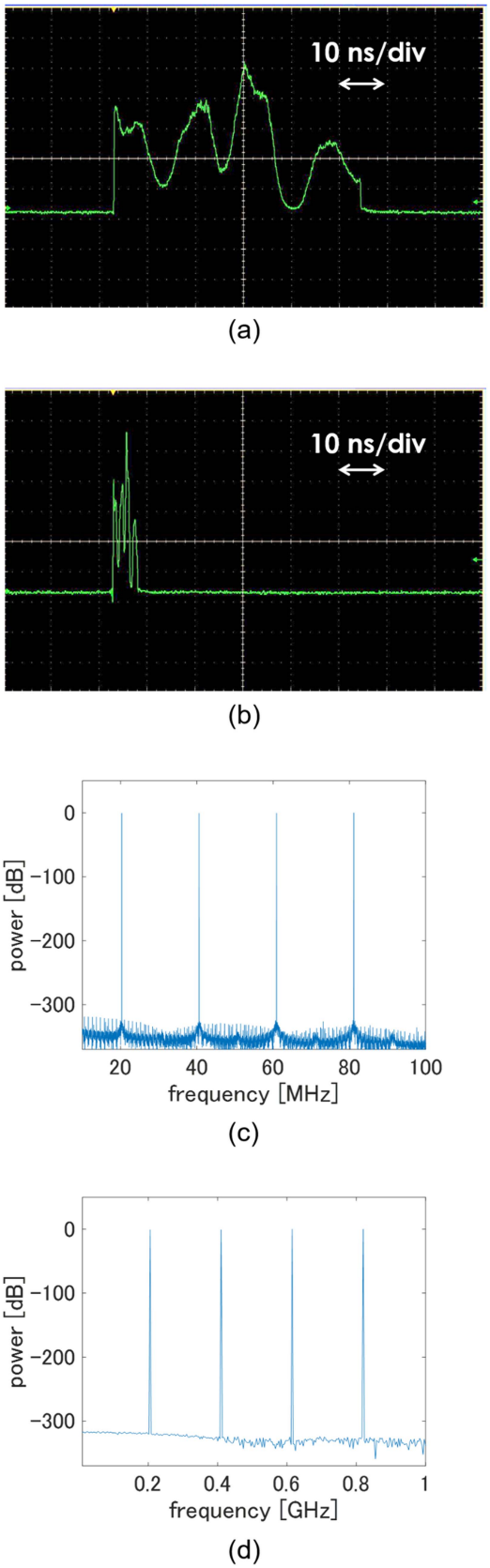

Fig. 9. Measured waveforms of the (a) original QPSK-modulated optical OFDM signal, (b) compressed signal by a factor of 9.4, and FFT spectra of (c) original QPSK-modulated optical OFDM signal, (d) compressed signal by a factor of 9.4.

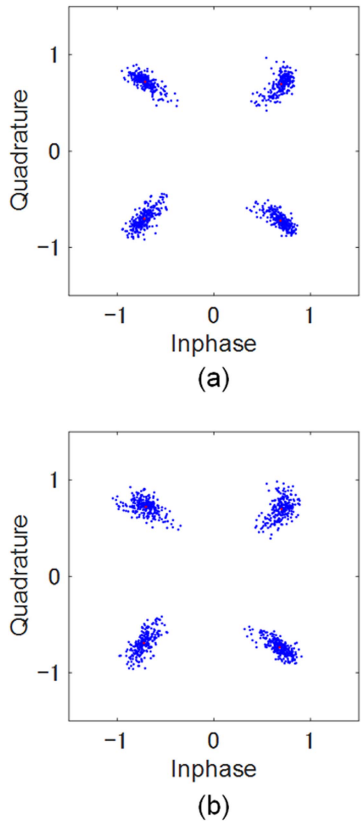

Fig. 10. Constellation diagrams of the measured waveforms (a) before and (b) after signal compression.

to the sum of OFDM subcarrier fields detuned from the central frequency ν_c.

The modulated stretched pulse in the MHz region is subsequently compressed to higher-frequency regions by two dispersion-compensating fibers with different dispersions of $+480$ ps/nm and $+1280$ ps/nm, respectively. The waveforms are measured by a digital oscilloscope (Tektronix DSA70404B) via a PD. Fig. 8 shows a measured waveform of a stretched pulse before superimposing a signal without an ideal flat shape. The unflattend pulse shape would be distorted the output signal but can be pre-compensated a synthesized signal before signal superimposing in the digital domain using the monitored unflattened pulse shape. In this experiment, since our AWG is not responding to such a real time operation, this distortion of the stretched pulse is post-compensated for signal quality evaluation using the differential value between the ideal and original waveforms.

Fig. 9(a) and (b) show the measured waveforms before and after signal compression of a QPSK-modulated optical OFDM signal for evaluating effective number of bit (*ENOB*) as one of signal quality metrics. In the QPSK-modulated optical OFDM signal, four QPSK phase shifts of 45°, 135°, 225°, and 315° are assigned in order of the frequency of the OFDM subcarrier. Since all compressed waveforms are measured one by one and each waveform is switched after waveform measurement, no spectral width broadening is observed in the spectra of QPSK signals. They agree well with the expected compressed ratio of

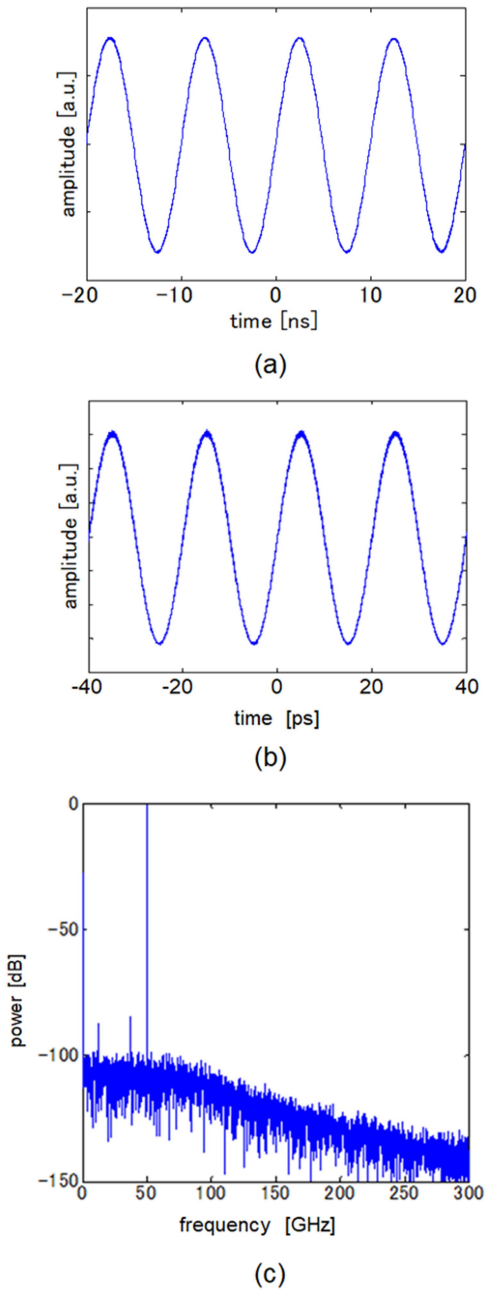

Fig. 11. Simulation results for achievable ENOB evaluation using ideal MHz-class modulation; waveforms (a) before and (b) after signal compression, (c) phase noise spectrum suffered from thermal and shot noises after signal compression and O/E conversion.

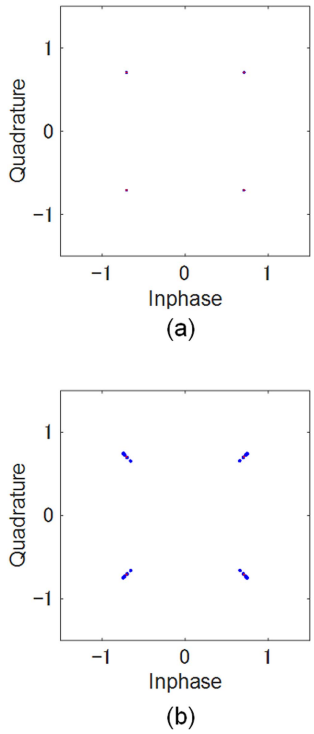

Fig. 12. Constellation diagrams of the waveforms (a) in digital domain and (b) after DCF-based compression.

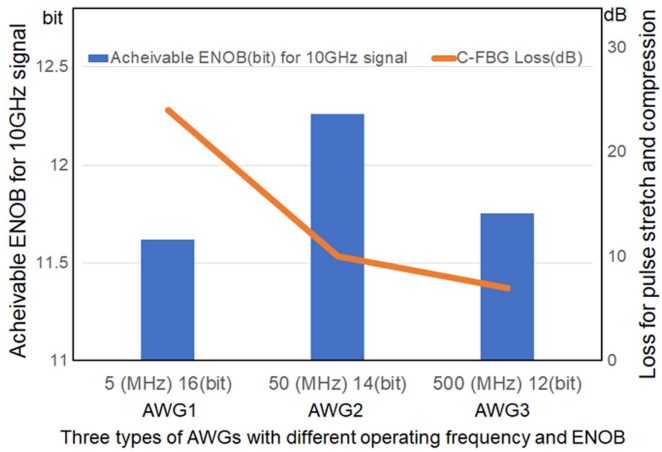

Fig. 13. Operating frequency dependencies of achievable ENOB for 10 GHz signal generation and C-FBG loss amount for different pulse stretch and compression.

9.4. The ENOB and signal-to-noise and distortion ratio (*SINAD*) are given by,

$$ENOB = (SINAD - 1.76)/6.02 \tag{2}$$

$$SINAD = (P_s + P_n + P_d)/(P_n + P_d), \tag{3}$$

where P_s, P_n, and P_d are the powers of signal, noise, and distortion, respectively. *ENOB* can be estimated from *SINAD*, measured over subcarriers and determined from the fast Fourier transform (FFT) spectrum of the measured signal, and Fig. 9(c) and (d) show the FFT spectra before and after signal compression. From these results, the *ENOB*s are evaluated to 4.836 bit and 4.718 bit, respectively. While the ENOB of the original signal before signal compression is not very high due to a severe distortion from the uncompensated nonlinearity of MZM at a low-frequency region, these results show that the signal quality is almost preserved after signal compression.

After all waveforms are measured one by one using an oscilloscope, the data symbols of 4 subcarriers are demodulated by Fourier transforming the measured waveforms because the superimposed signal E corresponds to the sum of OFDM subcarrier fields detuned from the central frequency ν_c. Fig. 10(a) and (b) display the constellation diagrams from the measured waveforms before and after signal compression to evaluate the

performance of QPSK modulation. From these constellation diagrams, the EVM values before and after signal compression are estimated to 12.64% and 13.64%, respectively. These results show that the signal quality is almost preserved after signal compression.

IV. Discussion

While recent electronics technology might not have serious problems in a few-GHz-order region but it is no longer simply scalable to the beyond GHz-order region. In fact, it is reported that around 1GHz would be the change-point from linear to exponential increase of power consumption [40]. On the other hand, this system has a potential to be scalable to the beyond GHz-order region but our experimental equipment unfortunately did not permit measurement in such a region; therefore, we evaluated the performance of signal generation in beyond GHz-order region by simulations.

A. Achievable ENOB Using Ideal MHz-Class Modulation

We assume the sinusoidal signal of 100 MHz generated from a low-frequency AWG and the AWG's ENOB is set to 16 bit which is the typical maximum ENOB in commercial MHz-class AWGs. The optical short pulse with 25-nm bandwidth radiating from the MLFL is first stretched to the MHz region by a dispersion element with the dispersion amount of -2000 ps/nm. The sinusoidally modulated stretched pulse in the MHz region is subsequently compressed into the sinusoidal signal of 50 GHz by another dispersion element with the dispersion of $+1996$ ps/nm, and the expected compressed ratio is given by 500. Fig. 11(a) and (b) show the waveforms before and after signal compression. Fig. 11(c) shows the phase noise spectrum suffering from thermal and shot noises after signal compression and O/E conversion. From Fig. 11(c), the ENOB is estimated as 12.38 bit. Despite the degradation and reduction from 16 to 12.38 bit, it could still retain high ENOB, which is competitive with the state-of-the-art of tens of GHz-class AWGs.

B. Achievable Signal Quality After Migration Using QPSK-Modulated Optical OFDM Signal in Beyond GHz Region

We examine the achievable signal quality performance after migration using QPSK-modulated optical OFDM signal in beyond GHz region by simulation. All 256 patterns waveforms corresponding to a QPSK modulated 4-subcarriers were digitally synthesized and compressed one by one. In this simulation, we synthesized an original OFDM signal with a 200 MHz carrier frequency and a 4MHz frequency interval so that a 50 GHz-band OFDM signal with a 1GHz frequency interval could be generated after 250-fold compression using a 25 nm-bandwidth optical pulse. Here, we assume a SMF with the dispersion amount of 12500 ps/nm and a DCF with a dispersion of -12450 ps/nm.for stretching and compressing, respectively. The compressed signals are detected by a PD and demodulated in OFDM standard demodulation to exploit the correlation between even and odd frequency components and Fourier transform. Fig. 12(a) and (b) display the constellation diagrams of original signals in digital domain and received signals after DCF-based compression, respectively. From these constellation diagrams, the EVM value after DCF-based compression are estimated to 474%. These results show that signal quality deterioration could be well prevented in beyond GHz region.

C. Appropriate Operating Frequency Region

Low-frequency AWGs and dispersing devices are critical devices that determine the achievable ENOB by the proposed method. In general, the lower the operating frequency of MHz-class AWGs decreases, the higher its ENOB increases. On the other hand, a chirped fiber Bragg grating (C-FBG) are often used as a large dispersion device, but stretching an optical pulse to several hundred ns, equivalent to a signal of several MHz, requires the cascaded use of many C-FBGs. As the number of required C-FBGs increases, insertion loss increases and degradation of the achievable ENOB by the proposed method increases. For example, insertion loss of more than 12 dB is caused in the case of a commercially available large-dispersion C-FBG of 10000 ps/nm which can stretch an optical pulse with a bandwidth of 20 nm to 200 ns equivalent to a 5 MHz signal. This suggests that there is a break-even point in the achievable ENOB and it determines the appropriate operating frequency region by the proposed method. Here, we estimate the achievable ENOB for 10 GHz signal generation when we employ three different types of MHz-class AWGs whose operating frequencies with their ENOBs are 5 MHz with 16 bit, 50 MHz with 14 bit, and 500 MHz with 12 bit. Fig. 13 shows the chart with two vertical axes for the achievable ENOB for 10 GHz signal generation on the left and the C-FBG loss amount for pulse stretch and compression on the right. From Fig. 13, the appropriate operating frequency of a MHz-class AWG would be 50 MHz to achieve the highest ENOB for 10 GHz signal generation.

V. Conclusion

In this paper, we firstly proposed a photonic-assisted arbitrary waveform generation for uplink applications in beyond 5G taking advantage of low frequency technology which can provide overwhelming competitiveness in analog resolution, cost, and power consumption except signal frequency. The photonic assistance for temporal waveform compression has a potential to upgrade signal frequency from MHz to more than tens GHz retaining the high ENOB of the low frequency technology and surpass the state of the arts of tens GHz class AWG. The principle of the proposed approach was verified in experiment and achievable ENOB is evaluated to over 12 bit at 50 GHz in simulation. The key to future improvement of the achievable ENOB in experiment is reduction of insertion loss in dispersion devices and compensation of nonlinearity of MZM at a low-frequency region.

Acknowledgment

The authors also would like to thank Enago for the English language review.

REFERENCES

[1] A. A. A. Boulogeorgos et al., "Terahertz technologies to deliver optical network quality of experience in wireless systems beyond 5G," *IEEE Commun. Mag.*, vol. 56, no. 6, pp. 144–151, Jun. 2018.

[2] S. Suyama et al., "A study on extreme wideband 6G radio access technologies for achieving 100 Gbps data rate in higher frequency bands," *IEICE Trans. Commun.*, vol. E104.B, no. 9, pp. 992–999, 2021.

[3] B. L. Shoop, *Photonic Analog-to-Digital Conversion*. Berlin, Germany: Springer-Verlag, 2001.

[4] G. C. Valley, "Photonic analog-to-digital converters," *Opt. Exp.*, vol. 15, pp. 1955–1982, 2007.

[5] A. Khilo et al., "Photonic ADC: Overcoming the bottleneck of electronic jitter," *Opt. Exp.*, vol. 20, no. 4, pp. 4454–4469, 2012.

[6] C. Laperle, "Advances in high-speed ADC, DAC, and DSP for optical transceivers," in *Proc. Opt. Fiber Commun. Conf. Expo. Nat. Fiber Opt. Eng. Conf.*, 2013, Art. no. OTh1F.

[7] T. Konishi et al., "Break even point analysis of photonic analog-to-digital conversion on power consumption," in *Proc. Eur. Conf. Opt. Commun.*, 2015, Art. no. We.1.6.2.

[8] Y. Sobu, S. Tanaka, Y. Tanaka, Y. Akiyama, and T. Hoshida, "High-speed, multi-level operation of all-silicon segmented modulator for optical DAC transmitter," in *Proc. IEEE Photon. Conf.*, 2020, pp. 1–2, doi: 10.1109/IPC47351.2020.9252254.

[9] C. Kress et al., "Analysis of the effects of jitter, relative intensity noise, and nonlinearity on a photonic digital-to-analog converter based on optical Nyquist pulse synthesis," *Opt. Exp.*, vol. 29, no. 15, pp. 23671–23681, 2021.

[10] T. Konishi et al., "All-optical analog-to-digital converter by use of self-frequency shifting in fiber and a pulse-shaping technique," *JOSA B*, vol. 19, pp. 2817–2823, 2002.

[11] T. Nishitani et al., "Optical coding scheme using optical interconnection for high sampling rate and high resolution photonic analog-to-digital conversion," *Opt. Exp.*, vol. 15, pp. 15812–15817, 2007.

[12] T. Nishitani, T. Konishi, and K. Itoh, "Resolution improvement of all-optical analog-to-digital conversion employing self-frequency shift and self-phase-modulation-induced spectral compression," *IEEE J. Sel. Topics Quantum Electron.*, vol. 14, no. 3, pp. 724–732, May/Jun. 2008.

[13] T. Nishitani et al., "Demonstration of 4-bit photonic analog-to-digital conversion employing self-frequency shift and SPM-induced spectral compression," in *Proc. Eur. Conf. Exhibit. Opt. Commun.*, 2007, Art. no. Th2.4.3.

[14] T. Konishi et al., "Five-bit parallel operation of optical quantization and coding for photonic analog-to-digital conversion," *Opt. Exp.*, vol. 19, pp. 16106–16114, 2011.

[15] T. Satoh, K. Takahashi, H. Matsui, K. Itoh, and T. Konishi, "10-GS/s 5-bit real-time optical quantization for photonic analog-to-digital conversion," *IEEE Photon. Technol. Lett.*, vol. 24, no. 10, pp. 830–832, May 2012.

[16] K. Takahashi et al., "Resolution upgrade toward 6-bit optical quantization using power-to-wavelength conversion for photonic analog-to-digital conversion," *Opt. Lett.*, vol. 38, no. 22, pp. 4864–4867, 2013.

[17] M. Hasegawa, T. Satoh, T. Nagashima, M. Mendez, and T. Konishi, "Below 100-fs timing jitter seamless operations in 10-GSamples/s 3-bit photonic analog-to-digital conversion," *IEEE Photon. J.*, vol. 7, no. 3, Jun. 2015, Art. no. 7201007.

[18] T. Nagashima, M. Hasegawa, and T. Konishi, "40 GSample/s all-optical analog to digital conversion with resolution degradation prevention," *IEEE Photon. Technol. Lett.*, vol. 29, no. 1, pp. 74–77, Jan. 2017.

[19] T. Konishi, Y. Yamasaki, Y. Kaihori, and R. Kamikawa, "Further development potential of photonic ADCs under contention among error terms in SNR," in *Proc. IEEE Photon. Soc. Summer Topicals Meeting Ser.*, 2020, pp. 1–2, doi: 10.1109/SUM48678.2020.9161055.

[20] T. Nishitani et al., "All-optical digital-to-analog conversion using pulse pattern recognition based on optical correlation processing," *Opt. Exp.*, vol. 13, no. 25, pp. 10310–10315, 2005.

[21] J. Oueis et al., "Uplink traffic in future mobile networks: Pulling the alarm," in *Proc. Int. Conf. Cogn. Radio Oriented Wireless Netw.*, May 2016, pp. 583–593.

[22] C. Bockelmann et al., "Massive machine-type communications in 5G: Physical and MAC-layer solutions," *IEEE Commun. Mag.*, vol. 54, no. 9, pp. 59–65, Sep. 2016.

[23] C. Kress et al., "Analysis of the effects of jitter, relative intensity noise, and nonlinearity on a photonic digital-to-analog converter based on optical Nyquist pulse synthesis," *Opt. Exp.*, vol. 29, no. 15, pp. 23671–23681, 2021.

[24] A. M. Weiner, "Femtosecond pulse shaping using spatial light modulators," *Rev. Sci. Instruments*, vol. 71, no. 5, pp. 1929–1960, 2000.

[25] J. Chou, Y. Han, and B. Jalali, "Adaptive RF-photonic arbitrary waveform generator," *IEEE Photon. Technol. Lett.*, vol. 15, no. 4, pp. 581–583, Apr. 2003.

[26] S. T. Cundiff et al., "Optical arbitrary waveform generation," *Nature Photon.*, vol. 4, no. 11, pp. 760–766, 2010.

[27] R. P. Scott et al., "Dynamic optical arbitrary waveform generation and measurement," *Opt. Exp.*, vol. 18, pp. 18655–18670, 2010.

[28] M. Li et al., "Recent progresses on optical arbitrary waveform generation," *Frontiers Optoelectron.*, vol. 7, no. 3, pp. 359–375, 2014.

[29] M. Tan et al., "Photonic RF arbitrary waveform generator based on a soliton crystal micro-comb source," *J. Lightw. Technol.*, vol. 38, no. 22, pp. 6221–6226, Nov. 2020.

[30] F. Coppinger, A. S. Bhushan, and B. Jalali, "Photonic time stretch and its application to analog-to-digital conversion," *IEEE Trans. Microw. Theory Techn.*, vol. 47, no. 7, pp. 1309–1314, Jul. 1999.

[31] J. Chou, J. A. Conway, G. A. Sefler, G. C. Valley, and B. Jalali, "Photonic bandwidth compression front end for digital oscilloscopes," *J. Lightw. Technol.*, vol. 27, no. 22, pp. 5073–5077, Nov. 2009.

[32] C. Wang, M. Li, and J. Yao, "Continuously tunable photonic microwave frequency multiplication by use of an unbalanced temporal pulse shaping system," *IEEE Photon. Technol. Lett.*, vol. 22, no. 17, pp. 1285–1287, Sep. 2010.

[33] C. Wang and Y. Jianping, "Fiber Bragg gratings for microwave photonics subsystems," *Opt. Exp.*, vol. 21, no. 19, pp. 22868–22884, 2013.

[34] C. Lim and A. Nirmalathas, "Radio-over-fiber technology: Present and future," *J. Lightw. Technol.*, vol. 39, no. 4, pp. 881–888, Feb. 2021.

[35] T. Konishi and Y. Kaihori, WO/2021/079710, 2021.

[36] T. Konishi, Y. Kaihori, M. Makino, and Y. Yamasaki, "Photonic-assisted digital-to-analog conversion taking advantage of low frequency technology," in *Proc. Int. Topical Meeting Microw. Photon.*, 2021, pp. 1–3, doi: 10.1109/MWP53341.2021.9639411.

[37] A. Mahjoubfar, D. V. Churkin, S. Barland, N. Broderick, S. K. Turitsyn, and B. Jalali, "Time stretch and its applications," *Nature Photon.*, vol. 11, no. 6, pp. 341–351, 2017.

[38] S. Gupta, D. R. Solli, A. Motafakker-Fard, and B. Jalali, "Capturing rogue events with the time-stretch recording scope," in *Proc. Eur. Conf. Lasers Electro-Opt.*, 2009, Art. no. CF6_1.

[39] A. S. Bhushan, F. Coppinger, and B. Jalali, "Time-stretched analogue-to-digital conversion," *Electron. Lett.*, vol. 34, no. 9, pp. 839–841, 1998.

[40] S. Rajagopal, "Power efficiency: The next challenge for multi-gigabit-per-second Wi-Fi," *IEEE Commun. Mag.*, vol. 52, no. 11, pp. 40–45, Nov. 2014.

Tsuyoshi Konishi (Senior Member, IEEE) received the B.E., M.E., and Dr. E. degrees in applied physics from Osaka University, Osaka, Japan, in 1991, 1993, and 1995, respectively.

He became an Assistant Professor with the Graduate School of Engineering, Osaka University, in 1996, and is currently an Associate Professor with the Division of Applied Physics. He stayed with Institut de Optique (France) as a Visiting Professor for his sabbatical term, in 2008 and 2009, respectively. His current research interests include ultrafast optical signal processing.

Dr. Konishi is currently serving as a Chair of IEEE photonics society Kansai chapter (IEEE PHO-36 Kansai Chapter) and a General Co-Chair of International Conference on Photonics in Switching and Computing 2022 (PSC 2022). He is a Senior Member of Optica and a Member of the Institute of Electronics, Information, and Communication Engineers (IEICE), the Japan Society of Applied Physics, and the Optical Society of Japan (OSJ).

Yuta Kaihori received the B.E. degree in applied physics and M.E. degree in material and life science from Osaka University, Osaka, Japan, in 2019 and 2021, respectively.

His research interests include optical signal processing and optical communication.

Masayuki Makino received the B.E. degree in applied physics from Osaka University, Osaka, Japan, in 2021, where he is currently working toward the M.E. degree in applied physics.

His research interests include optical signal processing and optical communication.